ACADEMIC PRESS

Available online at www.sciencedirect.com

SCIENCE DIRECT®

Journal of Sound and Vibration 265 (2003) 795–817

JOURNAL OF SOUND AND VIBRATION

www.elsevier.com/locate/jsvi

Free vibrations of laminated composite cylindrical shells with an interior rectangular plate

Young-Shin Lee*, Myung-Hwan Choi, Jae-Hoon Kim

Department of Mechanical Design Engineering, Chung-Nam National University, 220 Gung-Dong, Yuseong-gu, Daejeon 305-764, South Korea

Received 20 November 2001; accepted 9 August 2002

Abstract

The free vibration analysis of a laminated composite cylindrical shell with an interior rectangular plate is performed by the analytical and experimental methods. The frequency equations of vibration of the shell including the plate are formulated by using the receptance method. To obtain the free vibration characteristics before the combination of two structures, the energy principle based on the classical plate theory and Love's thin shell theory is adopted. The numerical results are compared with the results from an experiment, as well as a finite element analysis, to validate the current formulation. The influences of the length-to-radius ratio (L_S/a) and radius-to-thickness ratio (a/h_S) of the shell and fiber orientation angles (Θ) of symmetric cross- and angle-ply composite materials on the natural frequencies of a cylindrical laminated combined shell are also discussed in details.

1. Introduction

The cylindrical shells are often used in many structures, such as aerospace, marine, fuel tank and nuclear engineering applications. However, the actual structures in the engineering fields are combinations of basic elements such as beams, plates and shells. For example, an aircraft fuselage or a section of the submarine hull with a floor structure may be idealized as a combined shell of the plate and shell. When the plate and shell are jointed, the free vibration characteristics of these structures have a difference with those of simple components, and those are useful for the design of shell structures under various static and dynamic loads. In recent year, fiber reinforced composite materials have many industrial applications because of their advantages of high specific

*Corresponding author. Tel.: +82-42-821-6644; fax: +82-42-822-7366.
E-mail address: yslee@shell.cnu.ac.kr, leeys@cnu.ac.kr (Y.-S. Lee).

0022-460X/03/$ - see front matter
doi:10.1016/S0022-460X(02)01236-1

stiffness and specific strength properties. Thus, it is necessary to obtain the information about the vibrations of the laminated composite cylindrical shells with an interior rectangular plate.

The study of the vibrations for the composite cylindrical shells has been reported by many researchers [1–5]. They have studied the effects of various parameters such as boundary conditions, aspect ratios, fiber orientation angles and material properties of the composite shells on the vibration characteristics. But only several researchers investigated the vibrations of the combined shell with an interior plate. Peterson and Boyd [6] developed the analytical approach by using the Rayleigh–Ritz method to study the free vibration of a circular cylindrical shell partitioned by an interior rectangular plate. This paper was presented the effects of several parameters such as joint conditions between the plate and the shell, thickness of the structure and the position of the plate on the frequencies and the mode shapes of the combined shell. Irie et al. [7] studied the free vibration of non-circular cylindrical shells with longitudinal interior partitions by using the transfer matrix. Langley [8] applied a dynamic stiffness technique for the vibration analysis of a simply supported stiffened shell structure. Recently, Missaoui et al. [9] studied the free and forced vibration of a cylindrical shell with a floor partition based on a variational formulation in which the structural coupling is simulated using artificial spring systems.

Among various techniques to obtain the analytical solution, one of the useful approaches for analyzing the free vibration of combined structures is the receptance method discussed by Bishop and Johnson [10]. Azimi et al. [11] studied the natural frequencies and modes of continuous rectangular plates using the receptance method. Huang and Soedel [12] presented the results of an analysis of both ends of a simply supported cylindrical shell with a plate at an arbitrary axial position. Yim et al. [13] applied also this method to analyze the free vibration of clamped-free circular cylindrical shell with a plate attached at an arbitrary axial position. They obtained the frequency equation of the combined system by considering the continuity condition at the shell/plate joint, numerical results compared with these from a finite element (FE) analysis and vibration test.

In this paper, the receptance method is employed to analyze the free vibration of simply supported composite cylindrical combined shells with an interior rectangular plate. For two systems of the simply supported plate and shell, the natural frequencies and mode shape functions are obtained through the Rayleigh–Ritz procedure based on the energy principle. The classical plate theory and Love's thin shell theory is used. The analytical results are compared with those of the experiment and FE analysis using a FE program, ANSYS [14]. The influences of the number of layers, the fiber orientation angles, cross- and angle-ply laminated composite materials on the natural frequencies of the combined shell are also presented.

2. Analytical formulation

Fig. 1 shows the geometry and the co-ordinate systems of the circular cylindrical shell with an interior rectangular plate. The a, L_S and h_S are the radius, length and thickness of the shell, respectively. The b, L_P and h_P are the width, length and thickness of the plate. The displacement components of the plate and shell in each direction are presented as u_1^P, u_2^P, u_3^P and u_1^S, u_2^S, u_3^S, respectively. Where, superscripts S and P indicate the shell and the plate, respectively. The plate is attached at θ_1^* and θ_2^* position of the shell based on the vertical centerline.

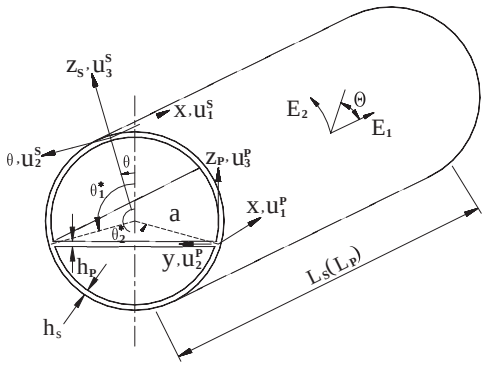

Fig. 1. Geometry of laminated composite cylindrical shell with an interior rectangular plate.

2.1. Free vibration of the rectangular plate

When the rectangular plate is attached at the interior space of the shell in the axial direction, one way of calculating the eigenvalues of the combined structure is the receptance method. With the receptance method, vibrational characteristics of the combined structure can be calculated from characteristics of the individual systems of the plate and the shell. Thus the natural frequencies and mode shape functions of an interior rectangular plate with simply supported boundary conditions are first obtained by using the classical plate theory.

Generally, $N_i = \{N_x, N_y, N_{xy}\}^{\mathrm{T}}$and $M_i = \{M_x, M_y, M_{xy}\}^{\mathrm{T}}$ are the resultant forces and moments of the laminated composite, and are written in terms of the middle surface extensional strains $\varepsilon_i = \{\varepsilon_1, \varepsilon_2, \varepsilon_{12}\}^{\mathrm{T}}$ and curvatures $\kappa_i = \{\kappa_1, \kappa_2, \kappa_{12}\}^{\mathrm{T}}$ as [15]

$$\left\{\frac{N_i}{M_i}\right\} = \left[\frac{A_{ij}\,|\,B_{ij}}{B_{ij}\,|\,D_{ij}}\right]\left\{\frac{\varepsilon_i}{\kappa_i}\right\}, \tag{1}$$

where

$$[A_{ij}, B_{ij}, C_{ij}] = \sum_{k=1}^{N}\int_{z_{k-1}}^{z_k} (\bar{Q}_{ij})_k (1, z, z^2)\,\mathrm{d}z. \tag{2}$$

In Eq. (2) A_{ij},B_{ij} and D_{ij} are extensional, coupling and bending stiffness matrixes, where the transformed reduced stiffnesses $\bar{Q}_{ij}$ are given in terms of the reduced stiffnesses Q_{ij}, including the fiber orientation angles and engineering constants. N refers to the number of total layers in plate and shell, z_k and z_{k-1} are the distances from the reference surface to the outer and inner surface of the kth layer as shown in Fig. 2.

The strain energy for transverse bending of a specially orthotropic laminated plate can be written in the form [16]

$$U_p = \frac{1}{2}\int_0^b \int_0^{L_p} [D_{11}u_{3,xx}^{P2} + 2D_{12}u_{3,xx}^{P}w_{,yy} + D_{22}u_{3,yy}^{P2} + 4D_{66}u_{3,xy}^{P2}]\,\mathrm{d}x\,\mathrm{d}y \tag{3}$$

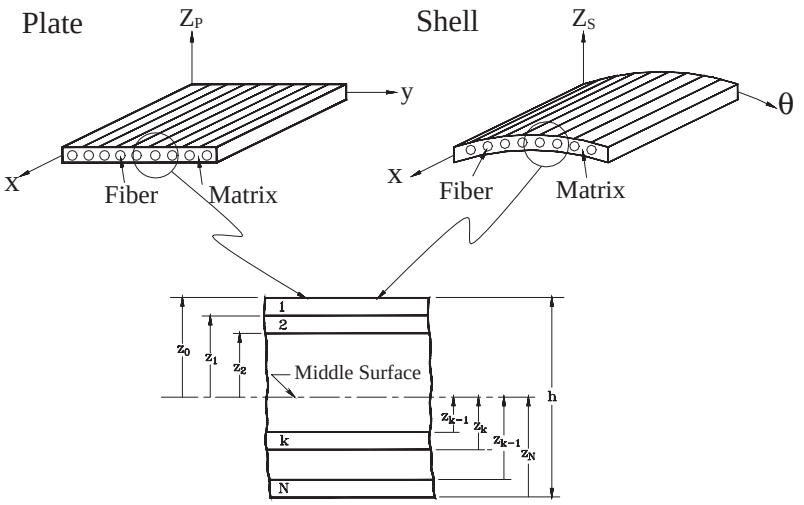

Fig. 2. Geometry of the n-layered laminate.

and the kinetic energy is given by

$$T_p = \frac{1}{2}\int_0^b \int_0^{L_p} \rho_{pt} u_{3,t}^{P2}\,\mathrm{d}x\,\mathrm{d}y, \tag{4}$$

where

$$\rho_{pt} = \sum_{k=1}^{N} \rho_{pk} h_{pk}, \tag{5}$$

u_3^p represents the displacement function of the plate in the normal direction, and $(\ )_{,x}$ represents partial differentiation with respect to x, etc. ρ_{pk} and h_{pk} are the density and the thickness of the kth layer of the laminated plate, respectively.

A general solution of the equation of motion, which satisfies the arbitrary boundary conditions, can be expressed as below:

$$\begin{aligned} u_3^P(x,y,t) &= U(x,y)\mathrm{e}^{\mathrm{j}\omega_{mn}t} \\ &= \sum_{m=1}^{m^*}\sum_{n=1}^{n^*} A_{mn} X_m(x)\, Y_n(y)\mathrm{e}^{\mathrm{j}\omega_{mn}t}, \end{aligned} \tag{6}$$

where A_{mn} are undetermined coefficients, ω_{mn} are the angular frequencies, and the $X_m(x)$ and $Y_n(y)$ are the beam functions satisfying the boundary conditions at the edges in the x and y directions. Substituting Eq. (6) into Eqs. (3) and (4), we obtain the energy terms. Then by applying the Rayleigh–Ritzs method, the total energy term can be minimized as

$$\frac{\partial}{\partial A_{mn}}(T_p - U_p) = 0 \quad \begin{cases} m = 1, 2, \ldots, m^*, \\ n = 1, 2, \ldots, n^* \end{cases} \tag{7}$$

and we obtain the frequency equation in the following matrix form:

$$\sum_{m=1}^{m^*}\sum_{n=1}^{n^*}[K_{mn}^{ij}-\omega_{mn}^2 M_{mn}^{ij}]A_{mn}=0 \quad \begin{cases} i=1,2,\ldots,m^*, \\ j=1,2,\ldots,n^*, \end{cases} \tag{8}$$

where

$$K_{mn}^{ij}=D_{11}I_3(m,i)J_1(n,j)+D_{12}[I_4(m,i)J_4(n,j)+I_4(m,i)J_1(n,j)] + D_{22}I_1(m,i)J_3(n,j)+4D_{66}I_2(m,i)J_2(n,j), \tag{9}$$

$$M_{mn}^{ij}=\rho_{pt}I_1(m,i)J_1(n,j), \tag{10}$$

I_i and J_i (i=1,2,3,4) are the integrals of the beam functions for the plate and given in Appendix A.

For the four edges simply supported plate, the displacement functions can be taken as sinusoidal functions

$$X_m(x)=\sin\frac{m\pi x}{L_p}, \tag{11a}$$

$$Y_n(y)=\sin\frac{n\pi y}{b}. \tag{11b}$$

Substituting Eq. (11) into the integral terms, the mass and stiffness matrix are obtained in Eqs. (9) and (10). Solving for the natural frequency from Eq. (8), the frequencies are given as

$$\omega_{mn}=\frac{\pi^2}{L_p^2\sqrt{\rho_p}}\sqrt{D_{11}m^4+2(D_{12}+2D_{66})m^2n^2R^2+D_{22}n^4R^4}, \tag{12}$$

where R is the plate aspect ratio L_p/b. In each case the mode shapes corresponding to those frequencies are

$$U_{3mn}(x,y)=\sin(m\pi x/L_p)\sin(n\pi y/b), \quad m,n=1,2,3\ldots. \tag{13}$$

2.2. Free vibration of the cylindrical shell

Similar to in case of the plate, the natural frequencies and mode shape functions of the simply supported cylindrical shell are obtained to apply the receptance method for combined structure. Those are calculated by Rayleigh–Ritz method based on the energy principle and Love's shell theory.

In general, in case of symmetric laminates with multiple specially orthotropic layers, the stiffnesses A_{16}, A_{26}, D_{16} and D_{26} are zero. Also, B_{ij} are zero because of symmetry. Since the symmetrically laminated shell with specially orthotropic in this study is considered, the strain energy of the laminated shell can be written in the following form:

$$U_s=\frac{1}{2}\int_0^{L_s}\int_0^{2\pi}[A_{11}\varepsilon_x^2+2A_{12}\varepsilon_x\varepsilon_\theta+A_{22}\varepsilon_\theta^2+A_{66}\varepsilon_{x\theta}^2 + D_{11}\kappa_x^2+2D_{12}\kappa_x\kappa_\theta+D_{22}\kappa_\theta^2+D_{66}\kappa_{x\theta}^2]a\,\mathrm{d}\theta\,\mathrm{d}x \tag{14}$$

and neglecting the rotary inertia moment, the kinetic energy of the shell is as follows:

$$T_s = \frac{1}{2}\int_0^{L_s}\int_0^{2\pi} \rho_{st}[(\dot{u}_1^s)^2 + (\dot{u}_2^s)^2 + (\dot{u}_3^s)^2]a\,\mathrm{d}\theta\,\mathrm{d}x. \tag{15}$$

The considered cylindrical shell is simply supported at both the axial ends. The mathematical expressions for this boundary condition are given by

$$u_2^S = u_3^S = M_1^S = N_1^S = 0 \quad \text{at } x = 0, \quad L_S. \tag{16}$$

The displacement functions which satisfies the boundary conditions at both ends are of the form

$$u_1^s(x,\theta,t) = \sum_{m=1}^{m^*}\sum_{n=1}^{n^*} U_{1mn}\bar{X}_m(x)\cos n\theta \mathrm{e}^{\mathrm{i}\omega_{mn}t}, \tag{17a}$$

$$u_2^s(x,\theta,t) = \sum_{m=1}^{m^*}\sum_{n=1}^{n^*} U_{2mn}X_m(x)\sin n\theta \mathrm{e}^{\mathrm{i}\omega_{mn}t}, \tag{17b}$$

$$u_3^s(x,\theta,t) = \sum_{m=1}^{m^*}\sum_{n=1}^{n^*} U_{3mn}X_{mn}(x)\cos n\theta \mathrm{e}^{\mathrm{i}\omega_{mn}t}, \tag{17c}$$

where $\bar{X}_m = \partial X_m/\partial x$, U_{imn} are the undetermined amplitude coefficients, and the m and n present a half wave numbers in the axial and circumferential directions, respectively. The X_m are the axial modal function satisfying the boundary conditions. One can use Eq. (11a) by replacing L_P with L_S. After energy terms are obtained in Eqs. (14) and (15), by applying the Rayleigh–Ritz procedure for the total energy, the frequency equation can be calculated as

$$|k_{ij} - \omega_{mn}^2 m_{ij}| = 0, \quad i,j = 1,2,3, \tag{18}$$

where ω_{mn} are the angular frequencies of the shell. The three natural modes that associated with the natural frequencies at each m,n combination can be expressed as below:

$$U_{1mn}^s(x,\theta) = (U_{1mn}/U_{3mn})\cos(m\pi x/L_s)\cos(n\theta), \tag{19a}$$

$$U_{2mn}^s(x,\theta) = (U_{2mn}/U_{3mn})\sin(m\pi x/L_s)\sin(n\theta), \tag{19b}$$

$$U_{3mn}^s(x,\theta) = \sin(m\pi x/L_s)\cos(n\theta). \tag{19c}$$

2.3. Free vibration of the combined structure

A receptance is defined [10,12,17] as the ratio of a displacement or slope response at a certain point to a harmonic force or moment input at the same or different point. For example, the simple case is two systems being joined through two co-ordinates as shown in Fig. 3. For system A the displacement (or slope) amplitudes X_{Ai} $(i = 1,2)$, as functions of harmonic force (or moment) amplitudes F_{Ai} $(j = 1,2)$ are

$$\{X_{Ai}\} = \{\alpha_{ij}\}^{\mathrm{T}}\{F_{Aj}\}. \tag{20}$$

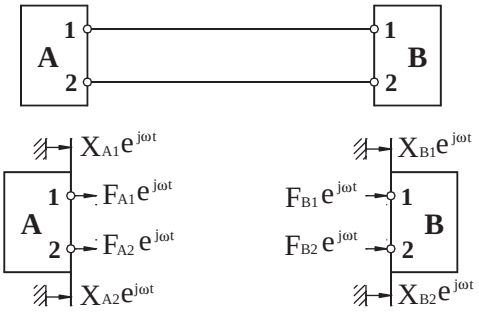

Fig. 3. Two systems jointed by two co-ordinates.

Similarly, for system B the outputs are

$$\{X_{Bi}\} = \{\beta_{ij}\}^{\mathrm{T}}\{F_{Bj}\}, \tag{21}$$

where α_{ij} and β_{ij} are the receptances of the shell and the plate, respectively.

When the two systems are joined and no forces (or moments) external to the two systems are applied, it must be equal because of displacement (or slope) continuity

$$\{F_{Aj}\} + \{F_{Bj}\} = 0 \tag{22}$$

and

$$\{X_{Ai}\} = \{X_{Bi}\}. \tag{23}$$

Combining these equations and applying the definitions of the receptance gives

$$[\alpha_{ij} + \beta_{ij}]\{F_{Aj}\} = 0. \tag{24}$$

For natural modes where $\{F_{Aj}\} \neq 0$, the natural frequencies of combined structure can be found from

$$|\alpha_{ij} + \beta_{ij}| = 0. \tag{25}$$

The term receptance is defined by the ratio of the response of a structure to the input function. Thus, if the input forcing function is defined, the response of the system and the receptance can be obtained. Once the receptances are calculated, the frequency equation can be derived by considering the continuity conditions at the joints. Fig. 4 shows the cross-sectional view of the displacements and the slopes at joining points due to the dynamic transverse line loads and line moments around the shell exerted by the motion of vibration.

By neglecting the damping of the system, the displacements of a structure subjected to dynamic loading can be expressed by the dynamic forcing function and the mode components of the plate and shell as an infinite series [17]

$$u_i(x, \theta, t) = \sum_{m=1}^{\infty}\sum_{n=1}^{\infty} \frac{F^*_{mn}}{(\omega^2_{mn} - \omega^2)} U_{imn}(x, \theta)e^{j\omega t}, \tag{26}$$

where ω_{mn} is the angular frequency of two independent systems which are calculated by Love's shell theory and classical plate theory. U_{imn} represents the mode components of the plate and the

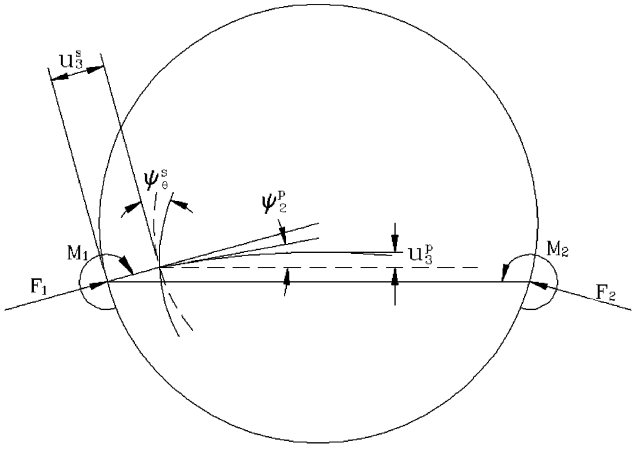

Fig. 4. Cross-sectional view of the displacements and the slopes at joining points.

shell in three principal directions. The dynamic forcing function F_{mn}^* can be obtained in Eq. (27), and the displacements of the plate and shell in Eq. (26) will be used later to calculate the receptances.

$$F_{mn}^* = \frac{1}{\rho h N_{mn}} \int_0^{2\pi} \int_0^{L_S} q_i^* U_{imn} a \, \mathrm{d}x \, \mathrm{d}\theta, \tag{27}$$

$$N_{mn} = \int_0^{2\pi} \int_0^{L_S} U_{imn}^2 a \, \mathrm{d}x \, \mathrm{d}\theta. \tag{28}$$

The input forcing functions, q_i^* $(i = 1, 2, 3)$ are the forces applied at two joints in the axial, circumferential and transverse normal directions.

In case of the rectangular plate attached at (x, θ_1^*) and (x, θ_2^*) positions of the cylindrical shell, the transverse dynamic excitation exerted at the joints due to the constraint of the displacements of the shell by the plate can be assumed as sinusoidal and Dirac delta function, δ:

$$q_3^*(x, \theta^*, t) = f_i^*(x, \theta^*, t) = F_i^S \sin(\bar{m}\pi x / L_S)\delta(\theta - \theta_i^*)\mathrm{e}^{\mathrm{j}\omega t}, \quad i = 1, 2, \tag{29}$$

where f_1^* and f_2^* are the transverse forcing functions applied on the shell at two joints in the circumferential direction. The transverse mode shape of the shell satisfying the simply supported boundary conditions is used as Eq. (19c) from neglecting the components in axial and circumferential directions in Eq. (19).

Substituting Eqs. (19c) and (27) into Eq. (26), in case of $\bar{m} = m$ the dynamic forcing function F_{mn}^* is found to be

$$F_{mn}^* = F_{mn}^*|_{F_1} + F_{mn}^*|_{F_2}, \tag{30}$$

where

$$F_{mn}^*|_{F_1} = \frac{F_1^S L_S}{2\rho_S h_S N_{mn}} \cos n\theta_1^*, \quad F_{mn}^*|_{F_2} = \frac{F_2^S L_S}{2\rho_S h_S N_{mn}} \cos n\theta_2^*, \tag{31}$$

$F_k^*|_{F_1}$ is the dynamic forcing function with only F_1 applied and $F_k^*|_{F_2}$ is one with only F_2 applied. Evaluation of Eq. (28), N_{mn} yields

$$N_{mn} = L_S a\pi/2. \tag{32}$$

Using Eqs. (26) and (30), the dynamic displacement of the shell can be represented using the mode summation as

$$u_3^S(x,\theta,t) = \frac{L_S}{2\rho_S h_S N_{mn}} \sum_{m=1}^{\infty}\sum_{n=1}^{\infty} \frac{(F_1^S \cos n\theta_1^* + F_2^S \cos n\theta_2^*)}{(\omega_{mn}^2 - \omega^2)} \sin(m\pi x/L_S)\cos n\theta e^{j\omega t}. \tag{33}$$

The circumferential slope of the shell can be obtained from Eq. (33) by differentiation with respect to the circumferential co-ordinate θ:

$$\psi_\theta^S(x,\theta,t) = -\frac{L_S}{2\rho_S h_S N_{mn}} \sum_{m=1}^{\infty}\sum_{n=1}^{\infty} \frac{n(F_1^S \cos n\theta_1^* + F_2^S \cos n\theta_2^*)}{(\omega_{mn}^2 - \omega^2)} \sin(m\pi x/L_S)\sin n\theta e^{j\omega t}. \tag{34}$$

Next, the dynamic moment loading exerted at two joints due to the constraint by the plate can be expressed as

$$T_\theta = m_i^*(x,\theta^*,t) = M_i^S \sin(\bar{m}\pi x/L_S)\delta(\theta - \theta_i^*)e^{j\omega t}, \quad i = 1,2, \tag{35}$$

where m_1^*, m_2^* are the moment functions applied at two joints in the circumferential position, $\theta = \theta_1^*$ and θ_2^*, respectively. The forcing functions due to the moment loading can be obtained from Ref. [17] as

$$F_{mn}^* = \frac{1}{\rho h N_{mn}} \int_0^{2\pi}\int_0^{L_S} U_{3mn}\left[\frac{1}{a}\left\{\frac{\partial(T_\theta)}{\partial\theta}\right\}\right] a\,dx\,d\theta. \tag{36}$$

Here, N_{mn} is the same as in Eq. (32). The displacement of the shell by moment loading can be obtained from Eqs. (26) and (36)

$$u_3^S(x,\theta,t) = \frac{L_S}{2\rho_S h_S N_{mn}} \sum_{m=1}^{\infty}\sum_{n=1}^{\infty} \frac{n(M_1^S \cos n\theta_1^* + M_2^S \cos n\theta_2^*)}{(\omega_{mn}^2 - \omega^2)} \sin(m\pi x/L_S)\cos n\theta e^{j\omega t}. \tag{37}$$

Using Eq. (37), the slope of shell by moment loading at the joints can be calculated as

$$\psi_\theta^S(x,\theta,t) = -\frac{L_S}{2\rho_S h_S N_{mn}} \sum_{m=1}^{\infty}\sum_{n=1}^{\infty} \frac{n^2(M_1^S \cos n\theta_1^* + M_2^S \cos n\theta_2^*)}{(\omega_{mn}^2 - \omega^2)} \sin(m\pi x/L_S)\sin n\theta e^{j\omega t}. \tag{38}$$

As a similar manner, one can consider the receptances for a rectangular plate simply supported at all edges with forces and moments exerted at two joints, (x, y_1^*) and (x, y_2^*). In this case, the dynamic excitation exerted at the joints due to the constraint of the displacements of the plate by the shell can be assumed as Eq. (39) using the Dirac delta and sinusoidal function.

$$f_i^*(x,y^*,t) = F_i^P \sin(\bar{m}\pi x/L_P)\delta(y - y_i^*)e^{j\omega t}, \quad i = 1,2. \tag{39}$$

Also, the mode shape function expressing the in-plane displacement of the simply supported plate can be assumed as

$$U_{2mn}^P = \sin(m\pi x/L_P)\cos(n\pi y/b). \tag{40}$$

Thus, the displacement of the plate can be expressed as below:

$$u_2^P(x,y,t)=\frac{2}{\rho_P h_P b}\sum_{m=1}^{\infty}\sum_{n=1}^{\infty}\frac{\{F_1^P\cos(n\pi y_1^*/b)-F_2^P\cos(n\pi y_2^*/b)\}}{(\omega_{mn}^2-\omega^2)}\cos(n\pi y/b)\sin(m\pi x/L_P)\mathrm{e}^{\mathrm{j}\omega t}. \quad (41)$$

To obtain the slope of a simply supported rectangular plate by edge moments, the transverse mode shape function can be used as that given in Eq. (19c). The periodic line moments excited at the joints, (x,y_1^*) and (x,y_2^*) can be expressed as below:

$$m_i^P(x,y^*,t)=M_i^P\sin(\bar{m}\pi x/L_P)\delta(y-y_i^*)\mathrm{e}^{\mathrm{j}\omega t},\quad i=1,2. \quad (42)$$

The transverse displacement of the plate by dynamic moments is

$$u_3^P(x,y,t)=-\frac{2\pi}{\rho_P h_P b^2}\sum_{m=1}^{\infty}\sum_{n=1}^{\infty}\frac{n\{M_1^P\cos(n\pi y_1^*/b)-M_2^P\cos(n\pi y_2^*/b)\}}{(\omega_{mn}^2-\omega^2)}\times\sin(n\pi y/b)\sin(m\pi x/L_P)\mathrm{e}^{\mathrm{j}\omega t}. \quad (43)$$

The slope of the plate in the width direction by dynamic moments can be obtained from Eq. (43) by differentiation with respect to the co-ordinate, y:

$$\psi_2^P(x,y,t)=-\frac{2\pi^2}{\rho_P h_P b^3}\sum_{m=1}^{\infty}\sum_{n=1}^{\infty}\frac{n^2\{M_1^P\cos(n\pi y_1^*/b)-M_2^P\cos(n\pi y_2^*/b)\}}{(\omega_{mn}^2-\omega^2)}\times\cos(n\pi y/b)\sin(m\pi x/L_P)\mathrm{e}^{\mathrm{j}\omega t}. \quad (44)$$

Finally, the receptances of the shell and the plate can be calculated using the definition of a receptance method, the displacements (and slopes) and the line forces (and moments), and are defined as following Eqs. (45) and (46), respectively,

$$\alpha_{(2i-1)(2j-1)}=\frac{u_{3i}^S(x,\theta_i^*,t)|_{F_j}}{f_j},\quad \alpha_{(2i)(2j-1)}=\frac{\psi_{\theta i}^S(x,\theta_i^*,t)|_{F_j}}{f_j},$$

$$\alpha_{(2i-1)(2j)}=\frac{u_{3i}^S(x,\theta_i^*,t)|_{M_j}}{m_j},\quad \alpha_{(2i)(2j)}=\frac{\psi_{\theta i}^S(x,\theta_i^*,t)|_{M_j}}{m_j},\quad i,j=1,2, \quad (45)$$

$$\beta_{(2i-1)(2j-1)}=\frac{u_{2i}^P(x,y_i^*,t)|_{F_j}}{(-1)^{(j-1)}f_j},\quad \beta_{(2i)(2j-1)}=\frac{\psi_{2i}^P(x,y_i^*,t)|_{F_j}}{(-1)^{(j-1)}f_j},$$

$$\beta_{(2i-1)(2j)}=\frac{u_{2i}^P(x,y_i^*,t)|_{M_j}}{(-1)^{(j-1)}m_j},\quad \beta_{(2i)(2j)}=\frac{\psi_{2i}^P(x,y_i^*,t)|_{M_j}}{(-1)^{(j-1)}m_j},\quad i,j=1,2. \quad (46)$$

In this study, only the slope of the plate in the width direction and the normal displacement of the shell due to dynamic forces are considered. The normal displacement of the plate and the slope of the shell in the circumferential direction due to dynamic moments are taken into consideration because the other components of displacement can be ignored. By applying the continuity

Table 1
Dimensions (mm) of combined composite shells

Material	Shell			Plate		
	Length (L_S)	Radius (a)	Thickness (h_S)	Length (L_P)	Width (b)	Thickness (h_P)
GFRP	360	109	3.5	360	218	3.5

condition at the joints, the frequency equation can be expressed as

$$\begin{bmatrix} \alpha_{11}+\beta_{11} & \alpha_{12}+\beta_{12} & \alpha_{13}+\beta_{13} & \alpha_{14}+\beta_{14} \\ \alpha_{21}+\beta_{21} & \alpha_{22}+\beta_{22} & \alpha_{23}+\beta_{23} & \alpha_{24}+\beta_{24} \\ \alpha_{31}+\beta_{31} & \alpha_{32}+\beta_{32} & \alpha_{31}+\beta_{33} & \alpha_{34}+\beta_{34} \\ \alpha_{41}+\beta_{41} & \alpha_{42}+\beta_{42} & \alpha_{43}+\beta_{43} & \alpha_{44}+\beta_{44} \end{bmatrix} \begin{Bmatrix} F_1 \\ M_1 \\ F_2 \\ M_2 \end{Bmatrix} = 0. \tag{47}$$

For the rectangular plate, neglecting the in-plane displacements due to moments, (u_2^P/M) give $\beta_{12}=\beta_{14}=\beta_{32}=\beta_{34}=0$. Similarly, the slopes in the normal direction due to forces (ψ_2^P/F) are also negligible, that is, $\beta_{21}=\beta_{23}=\beta_{41}=\beta_{43}=0$. Thus, from the condition of having non-trivial solution of Eq. (47), the frequency equation of the combined shell can be obtained as the following form:

$$\begin{vmatrix} \alpha_{11}+\beta_{11} & \alpha_{12} & \alpha_{13}+\beta_{13} & \alpha_{14} \\ \alpha_{21} & \alpha_{22}+\beta_{22} & \alpha_{23} & \alpha_{24}+\beta_{24} \\ \alpha_{31}+\beta_{31} & \alpha_{32} & \alpha_{31}+\beta_{33} & \alpha_{34} \\ \alpha_{41} & \alpha_{42}+\beta_{42} & \alpha_{43} & \alpha_{44}+\beta_{44} \end{vmatrix} = 0. \tag{48}$$

In Eq. (48) the receptances of the shell and the plate can be calculated as the ratio of a displacement (or slope) response at two joints to a harmonic force (or moment) input from Eqs. (45) and (46), and given in Appendix B.

3. Experiments

The combined shell specimens with an interior plate at the center of the shell are fabricated as plain weave glass/epoxy composites with $[0_3^\circ/\pm 45_3^\circ/90_3^\circ]_S$ stacking sequence. Table 1 presents the geometrical data of the composite combined shell, and the shell has the same length and thickness as the plate. The plate is attached at the center $(\theta_1^* = 90^\circ)$ of the shell and the same material properties as those of the shell. The material properties of the glass fiber reinforced plastic (GFRP) composites are obtained by uniaxial tensile tests using a strain gage and a universal testing machine, and as following:

$$E_1 = E_2 = 26.21\,\text{GPa}, \quad G_{12} = 4.91\,\text{GPa}, \quad \rho = 1880\,\text{kg/m}^3 \quad \upsilon_{12} = 0.12.$$

Fig. 5 shows the schematic view of the supporting devices to realize the simply supported boundary conditions of the shell and the plate at both ends. The cylindrical shell is supported by

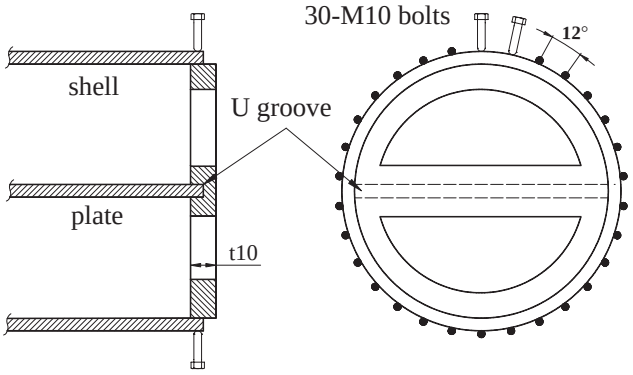

Fig. 5. Schematic view of supporting devices to realize simply supported boundary conditions.

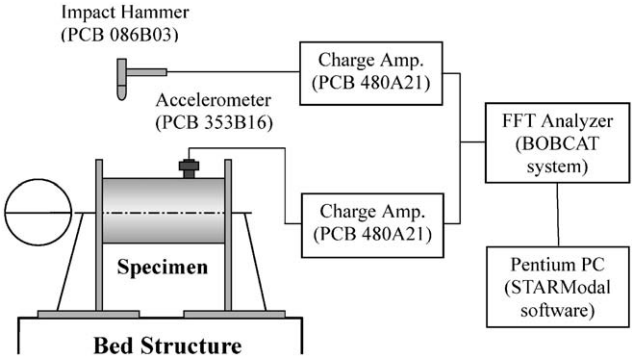

Fig. 6. Schematic diagram for the modal test.

using 30 bolts of 10 mm diameter with 12° equal spacing in the circumferential direction. To support the interior plate, the circular jig as shown in Fig. 5 is used, and it is made of acrylic with 10 mm thickness. The inside edge of the shell is supported by the outside edge of the circular jig, and the U groove in the middle supports the edge of an interior plate and constrains the displacements in the transverse direction. The circular jig has also open spaces to attach the accelerometer and to excite the plate using the impact hammer.

The principal equipments used in the experiment are an accelerometer (PCB 353B16), an impact hammer (PCB 086B03), a power supply amplifier (PCB 480A21) and a signal analyzer, etc. The vibration data are transmitted to the eight channel dynamic signal analyzer of Spectral Dynamics Inc., BOBCAT system connected by a Pentium PC allow data to be collected easily and transferred directly STAR Modal software. The experimental data are averaged with at least eight root mean square average schemes. The mode shapes are determined with measured displacements at total 52 grid points of the plate and the shell. The schematic diagram for the experimental modal testing is shown in Fig. 6.

Table 2
Comparison of the natural frequencies of analytical, experimental and ANSYS results of the GFRP plain weave composites cylindrical shell with interior plate at $\theta_1^* = 90^\circ$ location

Mode[a]	Method		
	Natural frequency (Hz)		
	Analysis	Experiment	FEM
First	234.5	245.0	241.6
Second	344.3	335.0	352.8
Third	547.2	540.0	547.5
Fourth	579.2	610.0	593.6
Fifth	696.0	660.0	614.5
Sixth	774.1	750.0	760.3
Seventh	804.5	810.0	803.5

[a] Frequency ascending order.

4. Results and discussion

To check the validity of the analytical approach results using the receptance method, the frequencies are compared with those from the experiment and a FE analysis. Table 2 presents the first seven natural frequencies of analytical, experimental and ANSYS results of the GFRP plain weave composites cylindrical shell with an interior plate at the center of the shell. The fundamental frequency of the combined shell is 234.5 Hz, and it shows the first bending mode of the interior plate. As shown in Table 2, the deviation between analytical and experimental results is about 4.3% for lowest fundamental frequency, and less than 7% for the other frequencies. Although the discrepancies between three methods are slight, the cause of the deviation is due to differences between ideal and actual boundary conditions of the plate and the shell in the experiment, and the relative coarseness of the meshes in the FE analysis. As a result, the analysis results are quite well agreed with those from the experiment and the FE analysis, showing the validity of the current formulation.

Fig. 7 shows the typical experimental and ANSYS mode shapes for the combined shell of the same model as listed in Table 2. These figures show a cross-section of the combined shell in the longitudinal and circumferential directions. The lowest frequency corresponds to a bending mode, which is basically governed by an interior plate motion. In case of the combined shell with the plate at the center of the shell the first four frequencies show the transverse bending modes of an interior plate with negligible motion of the shell. The shell mode appears first in the sixth frequency (750 Hz), in which one notices a slight deformation of the plate and a strong motion of the shell.

In following numerical results the effects of geometrical parameters (L_S/a, a/h_S) of the shell, stacking sequences and the number of layers (N), fiber orientation angles (Θ) and orthotropic ratios (E_1/E_2) are investigated for cross- and angle-ply laminated combined shells. In this study the shell and the plate have the same geometrical data ($L_S = L_P$, $h_S = h_P = 2$ mm) and the plate is

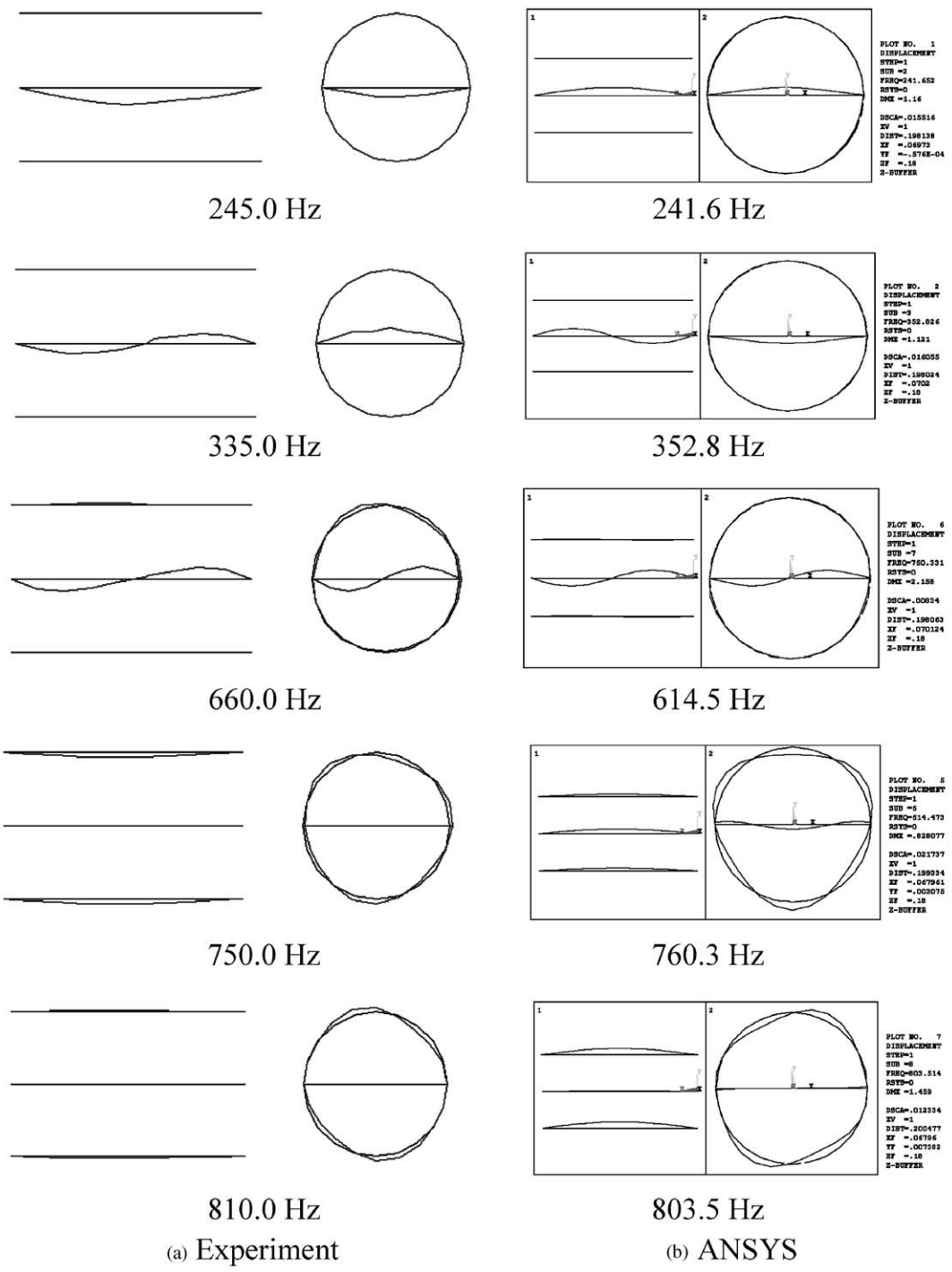

Fig. 7. Experimental and ANSYS mode shapes of the simply supported plain weave composites cylindrical shell with an interior plate at $\theta_1^* = 90^\circ$ location.

Table 3
Elastic properties of various composite materials

Properties	Unit	GFRP[18]	CFRP[18]
E_1	GPa	38.6	181.0
E_2	GPa	8.27	10.3
G_{12}	GPa	4.14	7.17
ρ	kg/m^3	1800	1600
v_{12}	—	0.45	0.26
E_1/E_2	—	4.67	17.57

Table 4
Influences of stacking sequences and the number of layers on the frequencies of CFRP symmetric cross-ply cylindrical combined shells; $L_S/a = 3$, $a/h_S = 50$

N[a]	Stacking sequence	Combined shell	Plate only	Shell only
3	[0/90/0]	179.0	146.4	1014.0
5	[0/90/0/90/0]	237.2	170.1	1156.2
7	[0/90/0/90/0/90/0]	259.9	180.6	1217.6
9	[0/90/0/90/0/90/0/90/0]	272.1	186.1	1250.0
15	[0/90/…/90/0]	288.5	194.0	1281.3
3	[90/0/90]	403.4	249.7	1353.1
5	[90/0/90/0/90]	372.2	234.1	1335.0
7	[90/0/90/0/90/0/90]	356.7	226.5	1325.4
9	[90/0/90/0/90/0/90/0/90]	347.3	222.0	1319.2
15	[90/0…/0/90]	334.0	215.0	1310.0

[a] N = the number of layers.

attached at the center, $\theta_1^* = 90^\circ$ of the shell. The considered stacking sequences are a four layered, cross-ply $[90^\circ/0^\circ]_S$ and angle-ply $[\Theta^\circ/-\Theta^\circ]_S$ cylindrical combined shells with symmetric laminates about the middle surface. Two composite materials from Ref. [18] are used and those properties are listed in Table 3, where $E_1/E_2 = 17.57$ for CFRP, $E_1/E_2 = 4.67$ for GFRP composite materials.

Table 4 shows the influence of stacking sequences and the number of layers on the fundamental frequencies of CFRP symmetric cross-ply cylindrical combined shells with $L_S/a = 3$, $a/h_S = 50$ and $h_S = 2$ mm. The thickness of one layer is varied in proportion to $2/N$ as N increases here. For two kinds of stacking sequences, the stacking sequence $[90^\circ/0^\circ\ldots]_S$ that is laminated by 90° angle at the outer surface has more high frequencies than $[0^\circ/90^\circ\ldots]_S$. The fundamental frequency of combined shell for $N = 3$ is shown to be the largest deviation about 56% between two stacking sequences. As listed in Table 4, the simply supported plate and shell with stacking sequence $[90^\circ/0^\circ\ldots]_S$ are also higher frequencies than in case of $[0^\circ/90^\circ\ldots]_S$. This phenomenon is because the number of 90° layer due to the symmetric stacking sequence $[90^\circ/0^\circ/90^\circ]$ is more than that of stacking sequence $[0^\circ/90^\circ/0^\circ]$, and it has an influence on the stiffness of the combined shell in the width (or circumferential) directions. But the deviations of frequencies between two stacking sequences decrease as N increases. This results show that the frequencies of the combined shell

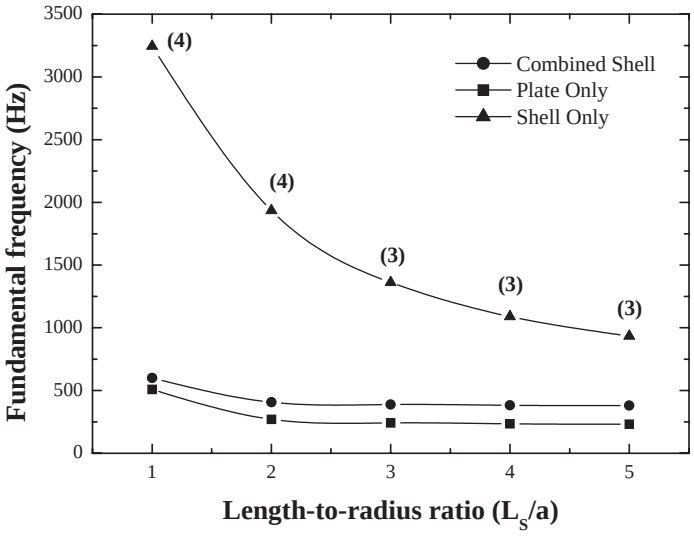

Fig. 8. Variation of fundamental frequencies for a four-layered, CFRP cross-ply $[90^\circ/0^\circ]_S$ combined shell with length-to-radius ratios(L_S/a); $a/h_S = 50$.

have significantly an effect on the lamination angle when the N is small, and the influence of 0°or 90° layers regardless of the stacking sequences decreases as the number of layers increases.

Fig. 8 presents the variation of fundamental frequencies for a four-layered, CFRP cross-ply $[90^\circ/0^\circ]_S$ cylindrical combined shell with various length-to-radius ratios(L_S/a). The shell can be considered as short shell ($L_S/a<5$) and the ratios are varied in the range from 1 to 5. The results are presented those of two individual structures before combination as well as the combined system together. Parenthesized numbers of the shell frequencies in Fig. 8 indicate the circumferential wave number (n) of the shell for the axial mode, $m = 1$. The fundamental frequencies for the combined shell decrease rapidly for the small L_S/a ratio. The circumferential wave number on the fundamental frequency decreases as the length of the shell increases. This is because the stiffness of the shell in the circumferential direction increases due to the increment of the shell length. That is, the circumferential mode, $n = 4$ is changed as $n = 3$ when the L_S/a increases. Also the natural frequencies of the plate only decrease with decreasing the L_S/a ratio, but if the L_S/a is about lager than 2.5, the frequencies of the plate only are not affected with the plate length. From the comparison of the results between two individual models before combination, the fundamental frequency of the combined system depends on the frequency of the plate mode, and is about 30% higher than that of the plate only.

The analysis results of the CFRP cross-ply $[90^\circ/0^\circ]_S$ combined shell with various radius-to-thickness ratios (a/h_S) are shown in Fig. 9. The fundamental frequencies of the combined shell decrease as the a/h_S ratio increases. In case of the $a/h_S = 30$, the frequency has a middle value of those between the plate and the shell with simply supported boundary conditions. But when the a/h_S ratio is large, the frequency of the combined shell is nearly the same with that of the plate only. This behavior is because the width of the plate due to the increment of the shell radius increases, so the stiffness of the interior plate is relatively weakened due to the variation of the

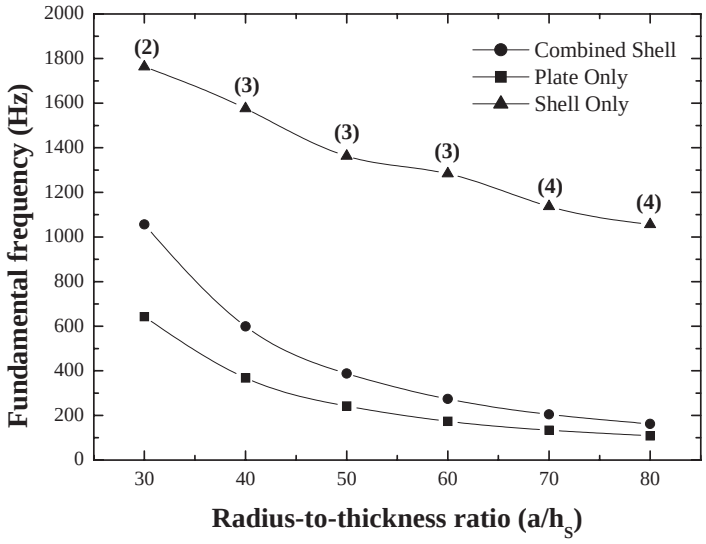

Fig. 9. Variation of fundamental frequencies for a four-layered, CFRP cross-ply $[90^\circ/0^\circ]_S$ combined shell with radius-to-thickness ratios(a/h_S); $L_S = L_P = 300$ mm.

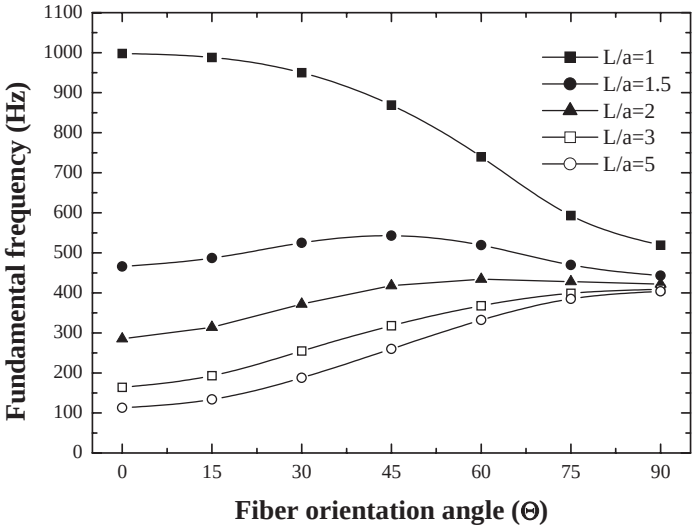

Fig. 10. Variation of fundamental frequencies for a four-layered, CFRP angle-ply $[\Theta^\circ/-\Theta^\circ]_S$ combined shell with fiber orientation angles and L_S/a ratios; $a/h_S = 50$.

geometrical dimension. The similar phenomena appear also on the behavior of the shell only. The circumferential mode of the shell is changed as $n = 4$ because the stiffness of the shell is weakened by increasing the radius.

Fig. 10 shows the influence of fiber orientation angles and L_S/a ratios of a four-layered, CFRP angle ply $[\Theta^\circ/-\Theta^\circ]_S$ cylindrical combined shell on the fundamental frequencies. When the shell is short ($L_S/a = 1$), the combined shell has the largest frequency at $\Theta = 0^\circ$, and those decrease as

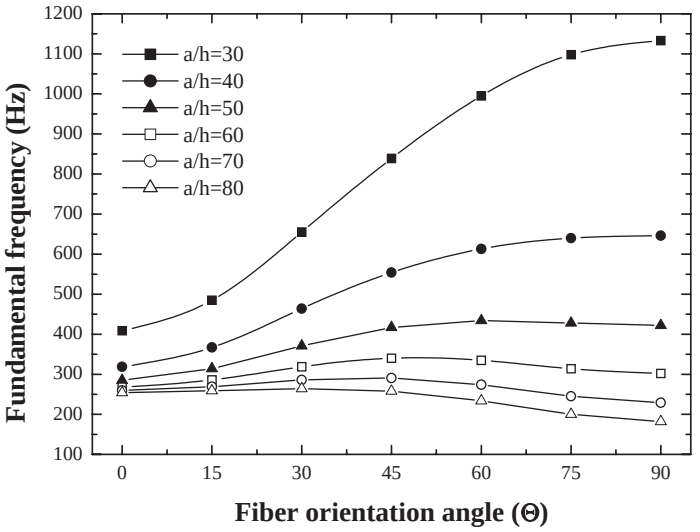

Fig. 11. Variation of fundamental frequencies for a four-layered, CFRP angle-ply $[\Theta^\circ/-\Theta^\circ]_S$ combined shell with fiber orientation angles and a/h_S ratios; $L_S = L_P = 200$ mm.

the Θ increases. This means that for the fixed radius ($a/h_S = 50$) the stiffness of the combined shell depends on the variation of the length and the lamination angle,$\Theta = 0^\circ$. Thus, the frequency has largely an influence on the variation of the shell length at $\Theta = 0^\circ$ in the axial direction. However, as the length of the shell increases, the fiber orientation angles showing the maximum frequency are changed from 0° to 90°, and when the L_S/a ratios are larger than 3, the highest frequencies occur at the $\Theta = 90^\circ$ because of the weaken of the stiffness in the axial direction.

The influence of fiber orientation angles and a/h_S ratios of a four-layered, CFRP angle ply $[\Theta^\circ/-\Theta^\circ]_S$ combined shell is shown in Fig. 11. The frequencies with increasing the a/h_S ratios decrease as the radius of shell increases because the width of the interior plate becomes large together. The combined shell in case of the $a/h_S = 30$ has the largest frequency at $\Theta = 90^\circ$, and those increase rapidly with increasing the Θ. The frequencies with a/h_S ratios are changed more at 90° than 0° contrary to the trend in Fig. 10. This is because the variation of the shell radius is more sensitive on the frequencies of the combined shell at $\Theta = 90^\circ$. But as the a/h_S ratios decrease, the fiber orientation angle showing the maximum frequency is changed from 0° to 90° as shown in Fig. 10.

Figs. 12 and 13 show the influence of fiber orientation angles on the fundamental frequencies of GFRP and CFRP angle-ply $[\Theta^\circ/-\Theta^\circ]_S$ combined shell with $L_S/a = 2$ and $a/h_S = 50$, respectively. The frequency of the plate only is the highest value at $\Theta = 45^\circ$ because the interior plate has the aspect ratio, $L_P/b = 1$. According to the increment of the Θ, the frequencies of the shell only decrease after the increment, and are the highest values at $\Theta = 60^\circ$ for GFRP and $\Theta = 45^\circ$ for CFRP material. The variation of the frequencies with the lamination angle is larger CFRP than GFRP material with small E_1/E_2. The frequencies of the combined shell are of a slightly higher value than those of the interior plate only, and the highest frequency is found at $\Theta = 60^\circ$. When the Θ is smaller than 45°, the difference of the fundamental frequency between the

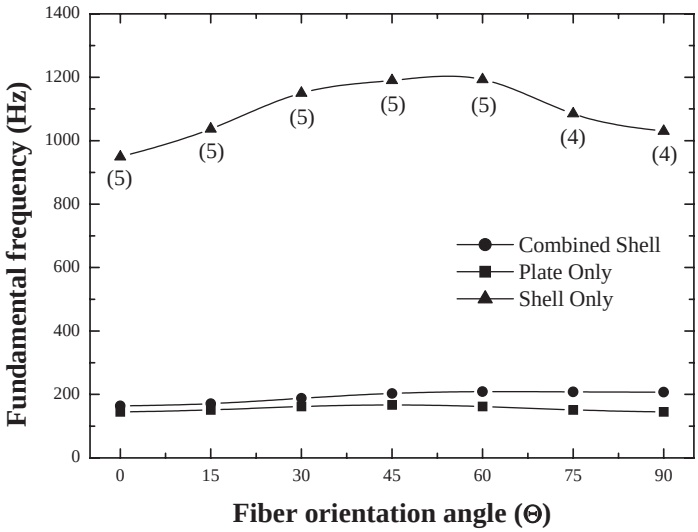

Fig. 12. Fundamental frequencies of a four-layered, GFRP angle-ply $[\Theta^\circ/-\Theta^\circ]_S$ combined shell with fiber orientation angles; $L_S/a = 2$, $a/h_S = 50$.

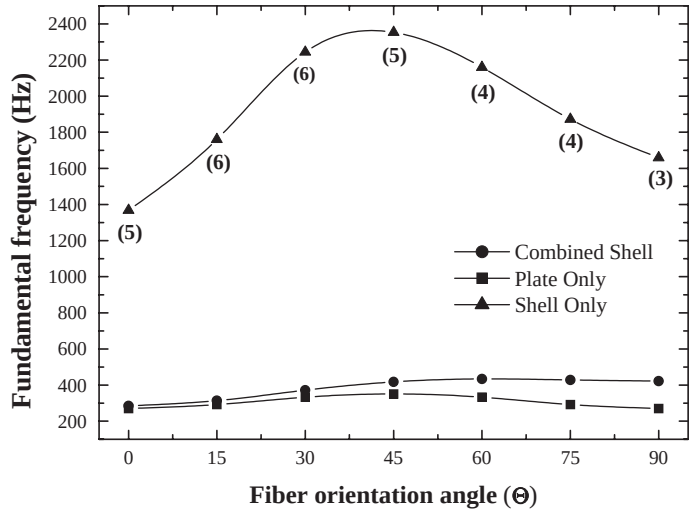

Fig. 13. Fundamental frequencies of a four-layered, CFRP angle-ply $[\Theta^\circ/-\Theta^\circ]_S$ combined shell with fiber orientation angles; $L_S/a = 2$, $a/h_S = 50$.

plate only and the combined shell is small, but is increased as the Θ increase. This reason is because the increment of the stiffness of the shell due to the increment of the lamination angle has an effect on the frequency of the combined shell. Also the lager the orthotropic modulus ratio, E_1/E_2 is, the larger the influence of fiber orientation angles on the natural frequencies of the combined shell is due to the variation of the stiffness of the interior plate and the shell in axial direction, although the influence of the E_1/E_2 ratio is not shown in detail here.

5. Conclusions

A frequency equation for the analysis of free vibration of laminated composite cylindrical shells with an interior rectangular plate is formulated using the receptance method. Numerical results of composite combined shells with simply supported boundary conditions are presented and are quite well agreed with those from the experiment and the FE analysis. When the line load and moment applied along the joints are assumed as sinusoidal function, the continuity conditions at the plate/shell joints are proven to be satisfied. The influence of various parameters on the frequency is also investigated in this paper. The fundamental frequency of the combined shell is highly dependent on the frequency of an interior rectangular plate showing the first bending mode. For two kinds of cross-ply laminate, the stacking sequence, $[90^\circ/0^\circ\ldots]_S$ that is laminated by 90° angle at the outer surface shows more high frequencies than in case of the $[0^\circ/90^\circ\ldots]_S$. As effects of geometrical parameters of the shell, when L_S/a and a/h_S ratios increase, the frequencies decrease due to the variation of the stiffness. Also when the shell is short, the frequencies of the combined shell are the highest values at the fiber orientation angle, $\Theta = 0^\circ$, but the lamination angle showing the maximum frequency is changed from 0° to 90°as the length of the shell increases.

Appendix A

The integrals of the beam functions for the plate are given as

$$I_1(m,n) = \int_0^{L_P} X_m X_n \,\mathrm{d}x, \quad I_2(m,n) = \int_0^{L_P} X_{m,x} X_{n,x} \,\mathrm{d}x,$$

$$I_3(m,n) = \int_0^{L_P} X_{m,xx} X_{n,xx} \,\mathrm{d}x, \quad I_4(m,n) = \int_0^{L_P} X_m X_{n,xx} \,\mathrm{d}x, \tag{A.1}$$

$$J_1(m,n) = \int_0^{b} Y_m Y_n \,\mathrm{d}y, \quad J_2(m,n) = \int_0^{b} Y_{m,y} Y_{n,y} \,\mathrm{d}y,$$

$$J_3(m,n) = \int_0^{b} Y_{m,yy} Y_{n,yy} \,\mathrm{d}y, \quad J_4(m,n) = \int_0^{b} Y_m Y_{n,yy} \,\mathrm{d}y. \tag{A.2}$$

Appendix B

The receptances of the shell in Eq. (48) are given as

$$\alpha_{11} = \frac{u_{31}^S(x,\theta_1^*,t)|_{F_1}}{f_1^S} = \frac{\dfrac{F_1^S L_S}{2\rho_S h_S N_{mn}} \sum_{m=1}^{\infty} \sum_{n=1}^{\infty} \dfrac{\cos n\theta_1^*}{(\omega_{mn}^2 - \omega^2)} \sin(m\pi x/L_S)\cos n\theta \mathrm{e}^{\mathrm{j}\omega t}}{F_1^S \sin(\bar{m}\pi x/L_S)\mathrm{e}^{\mathrm{j}\omega t}}$$
$$= SRC \cos n\theta_1^* \cos n\theta_1^*, \tag{B.1}$$

where if one lets

$$SRC = \frac{L_S}{2\rho_S h_S N_{mn}} \sum_{m=1}^{\infty} \sum_{n=1}^{\infty} \frac{1}{(\omega_{mn}^2 - \omega^2)},$$

$$\alpha_{31} = \frac{u_{32}^S(x, \theta_2^*, t)|_{F_1}}{f_1^S} = SRC \cos n\theta_1^* \cos n\theta_2^*, \tag{B.2}$$

$$\alpha_{13} = \frac{u_{31}^S(x, \theta_1^*, t)|_{F_2}}{f_2^S} = SRC \cos n\theta_1^* \cos n\theta_2^*, \tag{B.3}$$

$$\alpha_{33} = \frac{u_{32}^S(x, \theta_2^*, t)|_{F_2}}{f_2^S} = SRC \cos n\theta_2^* \cos n\theta_2^*, \tag{B.4}$$

$$\alpha_{21} = \frac{\psi_{\theta 1}^S(x, \theta_1^*, t)|_{F_1}}{f_1^S} = -SRC\, n \cos n\theta_1^* \sin n\theta_1^*, \tag{B.5}$$

$$\alpha_{41} = \frac{\psi_{\theta 2}^S(x, \theta_2^*, t)|_{F_1}}{f_1^S} = -SRC\, n \cos n\theta_1^* \sin n\theta_2^*, \tag{B.6}$$

$$\alpha_{23} = \frac{\psi_{\theta 1}^S(x, \theta_1^*, t)|_{F_2}}{f_2^S} = -SRC\, n \cos n\theta_2^* \sin n\theta_1^*, \tag{B.7}$$

$$\alpha_{43} = \frac{\psi_{\theta 2}^S(x, \theta_2^*, t)|_{F_2}}{f_2^S} = -SRC\, n \cos n\theta_2^* \sin n\theta_2^*, \tag{B.8}$$

$$\alpha_{12} = \frac{u_{31}^S(x, \theta_1^*, t)|_{M_1}}{m_1^S} = SRC\, n \sin n\theta_1^* \cos n\theta_1^*, \tag{B.9}$$

$$\alpha_{32} = \frac{u_{32}^S(x, \theta_2^*, t)|_{M_1}}{m_1^S} = SRC\, n \sin n\theta_1^* \cos n\theta_2^*, \tag{B.10}$$

$$\alpha_{14} = \frac{u_{31}^S(x, \theta_1^*, t)|_{M_2}}{m_2^S} = SRC\, n \sin n\theta_2^* \cos n\theta_1^*, \tag{B.11}$$

$$\alpha_{34} = \frac{u_{32}^S(x, \theta_2^*, t)|_{M_2}}{m_2^S} = SRC\, n \sin n\theta_2^* \cos n\theta_2^*, \tag{B.12}$$

$$\alpha_{22} = \frac{\psi_{\theta 1}^S(x, \theta_1^*, t)|_{M_1}}{m_1^S} = -SRC\, n^2 \sin n\theta_1^* \sin n\theta_1^*, \tag{B.13}$$

$$\alpha_{42} = \frac{\psi_{\theta 2}^S(x, \theta_2^*, t)|_{M_1}}{m_1^S} = -SRC\, n^2 \sin n\theta_1^* \sin n\theta_2^*, \tag{B.14}$$

$$\alpha_{24} = \frac{\psi^S_{\theta 1}(x, \theta^*_1, t)|_{M_2}}{m^S_2} = -SRC\, n^2 \sin n\theta^*_2 \sin n\theta^*_1, \tag{B.15}$$

$$\alpha_{44} = \frac{\psi^S_{\theta 2}(x, \theta^*_2, t)|_{M_2}}{m^S_2} = -SRC\, n^2 \sin n\theta^*_2 \sin n\theta^*_2. \tag{B.16}$$

Similarly, the receptances of the plate are defined as

$$\beta_{11} = \frac{u^P_{21}(x, y^*_1, t)|_{F_1}}{f^P_1} = \frac{\dfrac{2F^P_1}{\rho_P h_P b} \sum_{m=1}^{\infty} \sum_{n=1}^{\infty} \dfrac{\cos(n\pi y^*_1/b)}{(\omega^2_{mn} - \omega^2)} \cos(n\pi y/b) \sin(m\pi x/L_P) e^{j\omega t}}{F^P_1 \sin(\bar{m}\pi x/L_P) e^{j\omega t}}$$
$$= -PRC, \tag{B.17}$$

where if one lets

$$PRC = \frac{2}{\rho_P h_P b \omega^2},$$

$$\beta_{31} = \frac{u^P_{22}(x, y^*_2, t)|_{F_1}}{f^P_1} = PRC, \tag{B.18}$$

$$\beta_{13} = -\frac{u^P_{21}(x, y^*_1, t)|_{F_2}}{f^P_2} = -PRC, \tag{B.19}$$

$$\beta_{33} = -\frac{u^P_{22}(x, y^*_2, t)|_{F_2}}{f^P_2} = PRC, \tag{B.20}$$

$$\beta_{22} = \frac{\psi^P_{21}(x, y^*_1, t)|_{M_1}}{m^P_1} = -PRC\left(\frac{\omega\pi}{b}\right)^2 \sum_{m=1}^{\infty} \sum_{n=1}^{\infty} \frac{n^2}{(\omega^2_{mn} - \omega^2)}, \tag{B.21}$$

$$\beta_{42} = \frac{\psi^P_{22}(x, y^*_2, t)|_{M_1}}{m^P_1} = PRC\left(\frac{\omega\pi}{b}\right)^2 \sum_{m=1}^{\infty} \sum_{n=1}^{\infty} \frac{n^2}{(\omega^2_{mn} - \omega^2)}, \tag{B.22}$$

$$\beta_{24} = -\frac{\psi^P_{21}(x, y^*_1, t)|_{M_2}}{m^P_2} = -PRC\left(\frac{\omega\pi}{b}\right)^2 \sum_{m=1}^{\infty} \sum_{n=1}^{\infty} \frac{n^2}{(\omega^2_{mn} - \omega^2)}, \tag{B.23}$$

$$\beta_{44} = -\frac{\psi^P_{22}(x, y^*_2, t)|_{M_2}}{m^P_2} = PRC\left(\frac{\omega\pi}{b}\right)^2 \sum_{m=1}^{\infty} \sum_{n=1}^{\infty} \frac{n^2}{(\omega^2_{mn} - \omega^2)}. \tag{B.24}$$

References

[1] B. Baharlou, A.W. Leissa, Vibration and buckling of generally laminated composite plates with arbitrary edge conditions, International Journal of Mechanical Sciences 29 (1987) 545–555.

[2] A. Nosier, J.N. Reddy, Vibration and stability analyses of cross-ply laminated circular cylindrical shells, Journal of Sound and Vibration 157 (1992) 139–159.

[3] Y.S. Lee, Y.W. Kim, Vibration analysis of the rotating composite cylindrical shells with orthogonal stiffeners, Computers and Structures 69 (1998) 271–281.
[4] K.Y. Lam, C.T. Loy, Influence of boundary conditions and fiber orientation on the frequencies of thin orthotropic laminated cylindrical shells, Composite Structures 31 (1995) 21–30.
[5] K.Y. Lam, W. Qian, Free vibration of symmetric angle-ply thick laminated composite cylindrical shells, Composites Engineering, Part B 31B (2000) 345–354.
[6] M.R. Peterson, D.E. Boyd, Free vibrations of circular cylinders with longitudinal, interior partitions, Journal of Sound and Vibration 60 (1978) 45–62.
[7] T. Irie, G. Yamada, Y. Kobayashi, Free vibration of non-circular cylindrical shells with longitudinal interior partitions, Journal of Sound and Vibration 96 (1984) 133–142.
[8] R.S. Langley, Adynamic stiffness technique for the vibration analysis of stiffened shell structures, Journal of Sound and Vibration 156 (1992) 521–540.
[9] J. Missaoui, L. Cheng, M.J. Richard, Free and forced vibration of a cylindrical shell with a floor partition, Journal of Sound and Vibration 190 (1995) 21–40.
[10] R.E.D. Bishop, D.C. Johnson, The Mechanics of Vibration, Cambridge University Press, London, 1960.
[11] S. Azimi, J.F. Hamilton, W. Soedel, The receptance method applied to the free vibration of continuous rectangular plates, Journal of Sound and Vibration 93 (1984) 9–29.
[12] D.T. Huang, W. Soedel, Natural frequencies and mode shapes of a circular plate welded to a circular cylindrical shell at arbitrary axial positions, Journal of Sound and Vibration 163 (1993) 403–427.
[13] J.S. Yim, D.S. Shon, Y.S. Lee, Free vibration of clamped-free circular cylindrical shell with a plate attached at an arbitrary axial position, Journal of Sound and Vibration 213 (1998) 75–88.
[14] ANSYS Inc. 1996 ANSYS User's Manual, SAS IP, Inc.
[15] R.M. Jones, Mechanics of Composite Material,, Hemisphere Publishing Co., New York, 1975.
[16] J.M. Whitney, Structural Analysis of Laminated Anisotropic Plates, Technomic Publishing Co., Pennsylvania, 1987.
[17] W. Soedel, Vibrations of Shells and Plates, 2nd Edition, Marcel Dekker, Hong Kong, 1993.
[18] S.W. Tsai, Composite Design, Think Composite, Ohio, 1988.